ACS Catalysis

RESEARCH ARTICLE

pubs.acs.org/acscatalysis

Structural and Electrochemical Studies of Pt Clusters Supported on High-Surface-Area Tungsten Carbide for Oxygen Reduction

Ying Liu and William E. Mustain*

Department of Chemical, Materials and Biomolecular Engineering, University of Connecticut, Storrs, Connecticut 06269, United States

Supporting Information

ABSTRACT: High-surface-area tungsten carbide (WC) was synthesized via a molten solvent route and investigated as a noncarbon electrocatalyst support for nanosized Pt clusters. Pt clusters less than ~3 nm in size with a small particle size distribution were homogeneously deposited on the WC support by galvanic displacement with Cu. The activity of supported Pt clusters for the oxygen reduction reaction in acid media was studied. It was found that the activity of the Pt clusters is enhanced on WC compared with Pt clusters supported on carbon, and the most likely cause of this enhancement is electron transfer between the catalyst and support. The electrochemical stability of both raw and platinized WC was investigated by cyclic voltammetry, and the surface composition of the support was probed by X-ray photoelectron spectroscopy. It was found that WC is electrochemically stable at potentials less than 0.8 V vs the normal hydrogen electrode. At elevated potentials, the WC surface was oxidized to at least two different WO_x species during electrochemical treatment. This transformation of the dominant surface species as well as the tungsten coordination and bonding caused the detachment of Pt clusters from the support surface, which facilitated the agglomeration of Pt clusters on the electrocatalyst support surface.

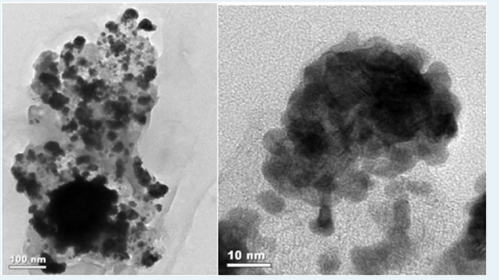

KEYWORDS: tungsten carbide, electrocatalyst, Pt clusters, cyclic voltammetry, X-ray photoelectron spectroscopy

1. INTRODUCTION

The oxygen reduction reaction (ORR) is an important electrochemical process that is active in low-temperature fuel cells,[1] oxygen sensors, metal−air batteries,[2] and the production of hydrogen peroxide.[3] In the proton exchange membrane fuel cell (PEMFC), the ORR is the performance-limiting reaction, even for state-of-the-art Pt and Pt alloy electrocatalysts[4−8] supported on high-surface-area carbon. Here, the sluggish ORR shows overpotentials nearing 300 mV, even at very low current.[9] Thus, a significant effort is currently underway to find high-activity ORR electrocatalysts. Several approaches have been attempted, including alloying Pt with non-noble metals[10−12] and depositing thin monolayer Pt films on other noble metals, such as Pd;[13] these have shown increased ORR activity, although troubles with chemical stability have stunted their widespread use in commercial systems.[14] An alternative approach that has recently gained popularity is utilizing synergistic effects between Pt and non-carbon supports to increase ORR activity.[15−17] Non-carbon supports provide an enhanced opportunity for bonding and electron transfer that graphitic supports do not because of carbon's saturated sp^2 surface bonding, which limits the interaction between Pt and support to simple van der Waals attraction.

Tungsten carbide (WC) has been intensively studied since Levy and Boudart discovered that it possesses catalytic properties similar to those of platinum group metals for several chemical reactions.[18] Since then, researchers have found that WC shows exceptionally high activities, similar to those of precious metal catalysts, for a number of reactions, including nitrophenol oxidation[19,20] and hydrogen evolution.[21−23] In electrocatalytic processes, WC has also shown some activity for the ORR.[23,24] WC has also been investigated as an electrocatalyst for the methanol oxidation reaction.[25−27] Although the performance of tungsten carbide is inferior in direct comparison to platinum,[28] its low price and insensitivity to catalyst poisons such as H_2S and CO make it an interesting alternative to the noble metal catalyst.[29]

Although the first results of the use of WC as PEMFC catalyst are promising, they are only the beginning. Many issues remain to be addressed, and it can be expected that by tailoring the electrocatalyst properties (i.e., structural, physical, and chemical bulk and surface properties) a considerable improvement in the electrocatalytic behavior and fuel cell performance can be achieved. One possible enhancement route is to utilize WC as an electrocatalyst support for highly dispersed Pt clusters. Recently, Pt/WC catalysts were shown to have higher activity than Pt/C electrocatalysts in a PEMFC.[30] Here, it was suggested that electron transfer between Pt and WC led to a rearrangement of the Pt d-band, which has an effect similar to alloying Pt with non-noble metals.

One limitation of previous studies utilizing WC is that the Pt electrocatalysts were prepared by simply mixing carbon

Received: December 13, 2010
Revised: January 11, 2011
Published: February 10, 2011

Table 1. Reactant Ratios for the Synthesis of WC Supports (1300 °C, 2 h)

	relative reactant concentrations			
sample no.	WO_3	C	KCl	Ni
1	1.0	4.0	0.07	0.02
2	1.0	4.0	1.0	0.02
3	1.0	4.0	1.0	0.0
4	1.0	1.5	1.0	0.02
5	1.0	3.0	1.0	0.02
6	1.0	3.5	1.0	0.02
7	1.0	5.0	1.0	0.02

supported WC with commercial Pt black and Pt/C.[31] This approach did not allow for extensive interaction between Pt and WC. In addition, the use of low surface area tungsten carbides limits their application as electrocatalyst support materials in PEMFCs. In addition, electrocatalyst performance is strongly dependent on its surface composition and structure. It has been shown that previous WC/C has a high concentration of graphitic carbon on its surface that suppresses electrocatalytic activity.[32−34] It has also been shown that there may be a high concentration of tungsten oxides on the WC surface, which have a significant influence on the properties of the electrocatalyst.

In the present work, the preparation of high-surface-area tungsten carbide crystals was realized by the aid of solid powder reagents in a molten solvent and a simple furnace treatment, similar to a method reported to produce whiskers of TaC,[35] and the performance of raw WC and Pt/WC toward oxygen reduction reaction was investigated. The corresponding structural characteristics were determined by X-ray diffraction (XRD), scanning electron microscopy (SEM), transmission electron microscopy (TEM), energy dispersive X-ray spectroscopy (EDX), X-ray photon spectroscopy (XPS) and Brunauer−Emmet−Teller (BET) gas adsorption. Finally, the ORR activity and Pt/WC stability was investigated by cyclic voltammetry (CV) and linear sweep voltammetry, chronoamperometry, and polarization in a laboratory scale, 5 cm^2 PEMFC.

2. EXPERIMENTAL SECTION

Synthesis of High-Surface-Area Tungsten Carbide Crystals. WO_3 (99+%, Acros Organics), carbon powder (Vulcan XC-72R), KCl (Fisher), and Ni powder (99.9%, Alfa Aesar) were used as the starting materials[36] for the synthesis of high-surface-area WC supports. Two grams of WO_3 was used in each preparation batch. The relative amounts of WO_3, C, KCl, and Ni were adjusted in this study, yielding seven distinct samples, which are summarized in Table 1. The precursors were mixed and ground with a mortar and pestle for 30 min to ensure that the precursors were well mixed and in intimate contact. Next, the ground precursor mixture was placed in an alumina ceramic boat (CoorsTek), placed in a CM, Inc. Rapid Temperature tube furnace, and heated in an argon atmosphere at 1300 °C for 2 h. The temperature ramp rate was 120 °C/h. Then, the resulting powder was rinsed with 6 M HCl to remove the KCl and Ni catalyst. Finally, the solids were washed with copious amounts of 18 MΩ Millipore deionized water and dried at 80 °C.

Several experiments were performed to determine the influence of the heat treatment conditions on the synthesis product.

Table 2. WC Heat Treatment Conditions with WO_3/C/KCl/Ni = 1:4:1:0.02

	A	B	C	D	E	F	G	H
T/°C	900	1100	1300	1300	1300	1300	1350	1400
time/h	2	2	2	4	8	33	4	4

For these experiments, the reactant ratio was maintained at WO/C/KCl/Ni = 1:4:1:0.02 (sample 2 in Table 1). Various heat treatments were performed, summarized in Table 2, and the resulting samples will be referred to as samples A, B, C, D, E, F, G, and H.

Deposition of Pt on WC and WO_3. Pt/WC and Pt/WO_3 electrocatalysts were prepared by depositing Pt nanoparticles on WC/WO_3 via galvanic displacement of a Cu layer by Pt[37] in a three-electrode electrochemical cell in N_2 atmosphere to avoid the oxidation of Cu atoms in contact with O_2. First, the working electrode was covered with a Cu monolayer by underpotential deposition in which the electrode potential was cycled between 0.0 and 0.3 V in aqueous 0.05 M H_2SO_4/0.05 M $CuSO_4$ for 3 cycles at a sweep rate 50 mV/s. Then, the electrode was rinsed with copious amounts of 18 MΩ Millipore water to remove Cu^{2+} ions from the electrode. Next, the electrode was placed into a 0.001 M K_2PtCl_4 (Acros Organics), 0.05 M H_2SO_4 aqueous solution for 4 min. Pt deposition on the WC/WO_3 surface was verified by voltammetry, TEM, and EDX.

Physical Characterization of Tungsten Carbide Crystals and Pt/WC, Pt/WO_3 Catalysts. The bulk composition of the electrocatalyst supports was confirmed by XRD with a Bruker D8 Advance diffractometer system. The morphology and microstructure of the high-surface-area supports was investigated by scanning electron microscopy using a FE-SEM JEOL 6335F with an integrated EDX and transmission electron microscopy with a FasTEM JEOL 2010. EDX was used to confirm the presence of W, O, and C atoms on the surface of the WC crystals. A Micromeritics ASAP 2020 accelerated surface area and porosimetry analyzer was used to determine the BET specific surface area. Finally, XPS was performed with a Kratos AXIS-165 surface analysis system to investigate the surface composition of support materials.

Electrochemical Characterization of WC, Pt/WC and Pt/WO_3. Cyclic voltammograms (CVs), recorded at room temperature using an Ecochemie Autolab PGSTAT302N potentiostat, were conducted in a custom-built (Adams & Chittenden Scientific Glass) three-electrode electrochemical cell using a 5 mm glassy carbon electrode (GCE) as the working electrode. A Pt flag was used as the counter electrode, and a saturated calomel electrode was used as the reference electrode; however, all potentials are reported versus the normal hydrogen electrode. The GCE was polished to a mirror finish and washed ultrasonically with deionized water prior to each experiment. To disperse the synthesized WC/WO_3 on the working electrode, an ink slurry was prepared by mixing WC/WO_3 with DI water and sonicating for 20 min to make a uniform 0.2 mg/mL suspension. Then, 20 μL of the suspension was added dropwise onto the GCE with a micropipet and then dried in air for 60 min. Next, a thin layer of Nafion was deposited onto the WC/WO_3 layer by applying 20 μL of a 0.05 wt % Nafion solution (diluted with water from 5% Nafion solution by DuPont, DE520), to prevent WC/WO_3 detachment from the working electrode during electrochemical testing.

dx.doi.org/10.1021/cs100140s |ACS Catal. 2011, 1, 212–220

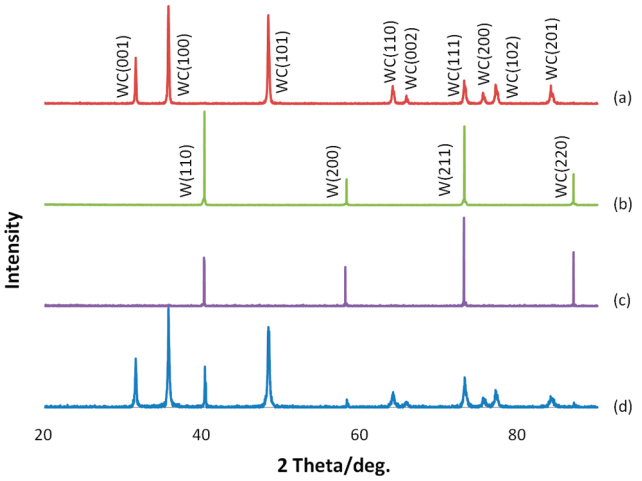

Figure 1. Powder XRD patterns for samples (a) 2, (b) 4, (c) 5, and (d) 6.

3. RESULTS AND DISCUSSION

3.1. Evaluation of Bulk Composition Using XRD. Powder XRD patterns of the synthesized crystals are shown in Figure 1. Phase identification was done using X'pert Highscore Plus. It was found that the ratio of bulk WC to W strongly depends on the initial molar ratio of tungsten oxide and carbon for the same carbonation temperature and time. When WO_3/C = 1:1.5 (sample 4) and 1:3 (sample 5), the bulk product was pure metallic tungsten, with no observable WC, W_2C, or WO_3. Their diffractograms are presented in Figure 1a and b, respectively. Here, the diffraction intensity of the (110) and (211) crystal faces were strong at 2θ = 40.43° and 73.12°, respectively. Two other weak intensity correspondence diffraction peaks, (200) at 2θ = 58.25° and (220) at 2θ = 87.01°, were observed.

At higher ratios, WO_3/C = 1:3.5 (sample 6), a mixture of tungsten and tungsten carbide was obtained, which is shown in Figure 1c. Finally, single-phase bulk WC was obtained at WO_3/C = 1:4 (sample 2), shown in Figure 1d. This reveals several possible pathways for tungsten carbide formation, which will be discussed in Section 3.3. For pure bulk WC, all of the primary peaks are observed and are labeled in Figure 1d.

Interestingly, none of the intermediate W_2C phase was observed in any of the prepared supports. Recently, Xiao et al.[38] reported that when WO_3 is carburized with ethane as the carbon source in the presence of Ni catalyst, pure W_2C is formed. In this method, C_2H_6 is first carburized to C, which then reacts with WO_3. The alkane carburization process contrasts with the one reported in this study considerably because it is limited by solid state diffusion of C into WO_3, where all of the reactants in this study have high mobility in the molten KCl phase during synthesis. Enhanced reactant mobility should provide more intimate contact between the reactants, which was reflected in the complete reaction to WC, as well as smaller crystal sizes, yielding higher surface area materials than reported previously.

3.2. Microstructure of As-Synthesized WC Electrocatalyst Supports. The specific surface area of the WC electrocatalyst supports was determined by BET, and the average value of several samples was 143 m^2/g (sample F, WO_3/C/KCl/Ni = 1:4:1:0.02, 1300 °C, 33 h), which is similar to that measured for Vulcan XC-72R (163 m^2/g) by our group previously.[39] This is significantly larger than commercial WC powder as well as those synthesized by other solid state methods,[40,41] which typically show specific surface areas of only a few dozen square meters per gram. This high surface area makes molten synthesized WC a promising support for Pt cluster electrocatalysts in PEMFCs.

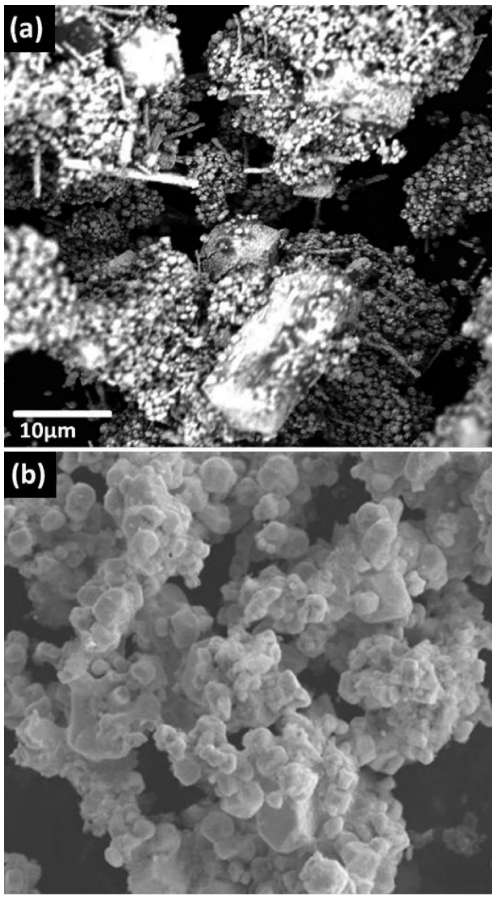

Figure 2. SEM images of pure bulk phase tungsten carbides (a) without and (b) with the Ni catalyst at 1300 °C, 33 h.

The particle structure and composition was studied using TEM, SEM, and EDX. TEM images (Supporting Information Figure S1) showed that the tungsten carbide crystals were not single spherical particles, but irregularly sized agglomerates. Each agglomerate was approximately 0.5−1 μm. This was also observed by SEM images for supports prepared with (Figure 2b) and without (Figure 2a) the Ni catalyst. Comparing the microstructures of the WC crystals shown in Figures 2a and 2b, it appears that the formation of homogeneous, high-surface-area WC was facilitated by adding Ni to the synthesis bath. Without Ni, though the product was pure WC, the shape and size of particles was highly irregular.

EDX was used to confirm the homogeneous dispersion of W and C on the support surface. Thus, a SEM image for WC is shown in Figure 3a, and the corresponding EDX maps for carbon, tungsten, and oxygen are shown in Figure 3b, c, and d, respectively. Since the WC was placed on carbon tape for SEM analysis, carbon was also seen in the gaps surrounding the support in Figure 3c. Otherwise, the signals for W and C overlap nicely. Surprisingly, a significant amount of elemental O is also observed on the support surface, despite no apparent WO_3 in any of the XRD spectra. One limitation of XRD stems from its large

dx.doi.org/10.1021/cs100140s |ACS Catal. 2011, 1, 212–220

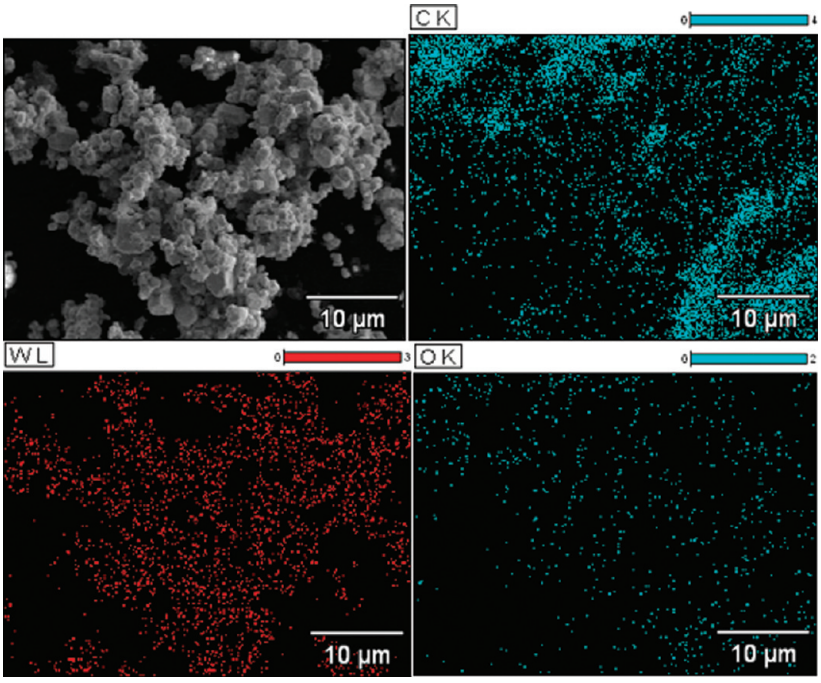

Figure 3. EDX images of tungsten carbides supports from (Ni/KCl)WO_3/C, 1300 °C, 2 h.

penetration depth (~1 μm), restricting its extensive use to identification of bulk structures. Since electrochemical processes occur exclusively on the surface, its composition is of primary importance and was probed by XPS.

3.3. Surface Characterization of Prepared WC. XPS was used in this study to investigate the influence of synthesis conditions on the surface composition of bulk phase WC supports. Here, the reactant ratio was held constant (WO_3/C/KCl/Ni = 1:4:1:0.02) while changing the heat treatment temperature and time per Table 2. For all samples, XRD was used to confirm that the bulk phase was WC. Five surface species were observed by XPS, although their relative amounts were a clear function of heat treatment: (i) WC; (ii) metallic W; (iii) atomic C; (iv) WO_3; and (v) a nonfully coordinated tungsten, whose signature was consistent with WO_2. The results are summarized in Figure 4. In all cases, the surface of the as-synthesized supports was dominated by WC, W, and C.

Generally, the surface concentration of WC increased with higher heat treatment temperature and decreased with treatment time. In addition, increased surface WC was mirrored by increasing surface metallic W and decreasing C, WO_3, and WO_2. However, SEM and BET results suggested that increasing the heat treatment temperature also increased the mean particle size and decreased the internal porosity, which are not advantageous for an electrocatalyst support. The presence of multiple WO_x species was surprising, because these materials were synthesized in an oxygen-free environment, and XRD did not detect any WO_3 remaining in the bulk. It is unlikely from the synthesis environment that WO_3 could be reduced to a less fully coordinated oxide. The most likely explanation for the presence of WO_x is that post-synthesis, the surface contains W, C, and WC only. Then, some of the metallic W is subsequently oxidized by exposure to air, the aqueous acid rinse step to remove the Ni catalyst, or both. This would yield approximately identical W and C contents on the surface postsynthesis with a simple trend of increasing WC content with temperature with decreasing W and C. This is confirmed by Figure 4 if the composition of W, WO_3, and WO_2 are summed.

The balance between the relative amounts of W, C, and WC as a function of synthesis temperature has been observed by several researchers[42,43] over many synthesis routes and treatment times. One interesting exception is nanostructured WC prepared by Liang et al., which was deposited on carbon nanotubes by microwave irradiation of solvated precursors, which yielded very small particles with low surface carbon, although mixtures of WC and W_2C were obtained.[44] This suggests that there is a bulk thermodynamic, not kinetic, limitation in the fabrication of WC crystals with a pure WC surface. Therefore, the free energy change for the primary routes for the formation of W and tungsten carbide from WO_3 and C proposed in the literature was investigated. These are shown in eqs 1−7:

$$WO_3 + 1.5C \leftrightarrow W + 1.5CO_2 \quad (1)$$

$$WO_3 + 2C \leftrightarrow 0.5W_2C + 1.5CO \quad (2)$$

$$WO_3 + 2.5C \leftrightarrow WC + 1.5CO_2 \quad (3)$$

$$WO_3 + 3C \leftrightarrow W + 3CO \quad (4)$$

$$WO_3 + 3.5C \leftrightarrow 0.5W_2C + 3CO \quad (5)$$

$$WO_3 + 4C \leftrightarrow WC + 3CO \quad (6)$$

$$W + C \leftrightarrow WC \quad (7)$$

The free-energy change for each reaction was calculated using eq 8 and is presented in Supporting Information Table S1 every 100 degrees between 900 and 1700 K.

$$\Delta G = \sum \nu_i G_i \quad (8)$$

dx.doi.org/10.1021/cs100140s |*ACS Catal.* 2011, 1, 212–220

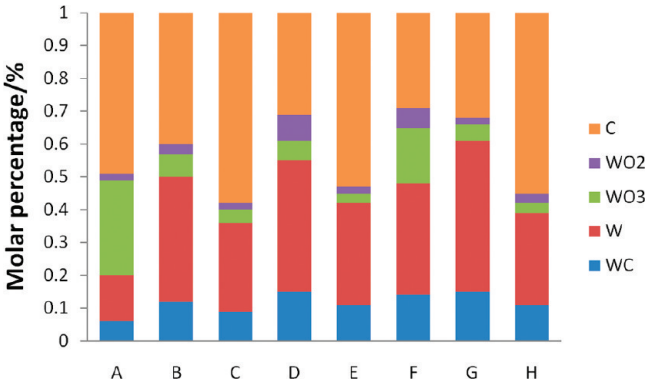

Figure 4. XPS results of the surface composition of tungsten carbide crystals with various heat treatment schemes.

Here, ν_i is the reaction stoichiometric coefficient and G_i is the Gibbs energy of formation at the given T and atmospheric pressure. The results in Supporting Information Table S1 suggest that eq 2 is essentially inactive over the entire temperature window in this study due to its extremely large, positive Gibbs energy of reaction, making eq 7 the least thermodynamically favored of the likely reactions. This suggests that the surface, even after synthesis, will consist of W, C, and WC, which at least qualitatively confirms the XPS results.

The thermodynamic limitation imposed by eq 7 does explain, albeit underestimate, the amount of surface W and C after synthesis. However, it is well established that continuum thermodynamics is poor in quantifying surface processes and their equilibrium. Thus, a more surface-sensitive thermodynamic approach should be used and is described below.

The surface excess concentration of an adatom B on a surface, Γ_B, is given by[45]

$$\Gamma_B = \frac{m_B}{A} \tag{9}$$

where m_B is the mass of B, and A is the surface area. The differential for the surface Gibbs free energy at constant temperature is

$$dG = A\, d\gamma + m_B\, d\mu_B \tag{10}$$

where γ is the surface tension and μ_B is the chemical potential of species B on the surface. At equilibrium, $dG = 0$ and the differential can be combined with eq 9

$$\Gamma_B = -\left(\frac{\partial\gamma}{d\mu_B}\right)_T \tag{11}$$

The surface chemical potential of species B is given by eq 12,

$$d\mu_B = RT\, d\ln x_B \tag{12}$$

where x_B is the mol fraction of B on the surface, R is the ideal gas constant, and T is the temperature. Hence,

$$\Gamma_B = -\frac{x_B}{RT}\left(\frac{\partial\gamma}{dx_B}\right)_T \tag{13}$$

Therefore, if the addition of B to a system lowers the surface tension (γ_B is smaller than γ), the segregation of component B to the surface is thermodynamically favored.

Recent first principles calculations by Knizhnik and co-workers[46] has shown that the surface tension of WC will be lowered with the addition of W and C on the surface, indicating the W and C are the preferred surface species. Thus, when the surface free energy is considered, it can be seen that both the dissociated W and C (eq 7) will segregate to the surface. This is the most likely explanation for the high W and C content on the surface post-synthesis and suggests that it is not thermodynamically feasible to obtain a stable, pure WC surface through bulk solid-state synthesis approaches. Thus, future synthesis methods for high-surface-purity WC should focus on either reducing the segregation driving force (i.e., through alloying or core−shell structures) or engineering low-coordination or low-crystallinity nanoparticles, in which the separation between surface and bulk phases is less clear.

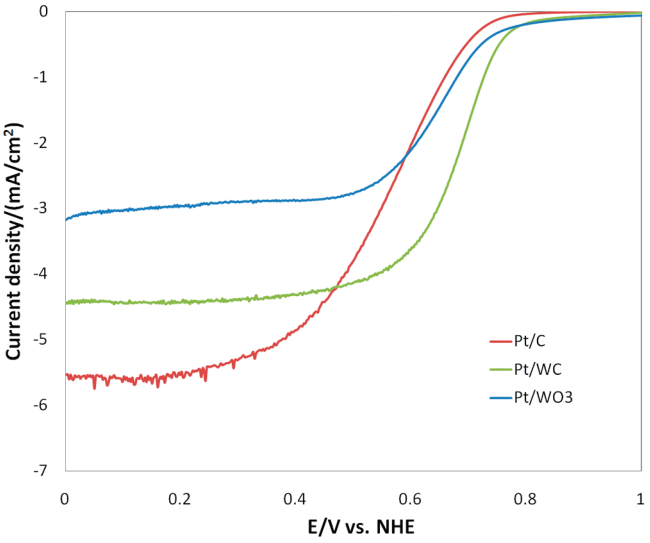

Figure 5. Linear sweep voltammograms for thin film Pt/C, Pt/WC, and Pt/WO_3 electrocatalysts in O_2-saturated 0.05 M H_2SO_4; 10 mv/s, 1600 rpm.

3.4. Oxygen Reduction Activity of Pt Clusters Supported on WC. Positive going linear sweep polarization curves are presented in Figure 5 for platinum clusters supported on Vulcan XC-72R (Pt/C), commercial WO_3 (Pt/WO_3), and sample F WC supports prepared in this study (Pt/WC). Pt/WO_3 showed a slight positive shift in the ORR onset and half-wave potentials compared with Pt/C, suggesting that Pt−OH formation is slightly delayed. However, the mass transport limiting current is nearly halved with identical loading and surface area, suggesting the formation of a significant amount of unwanted byproduct hydrogen peroxide from the incomplete reduction of O_2. However, it is unclear if this peroxide formation is caused by a shift in the ORR mechanism or the incomplete reduction of O_2 on WO_3 itself.

Pt/WC showed a significant improvement in ORR activity compared with Pt/C. This is evidenced by a large shift in both the ORR onset and half-wave potentials. The half-wave potential increased from 0.55 V on Pt/C to 0.72 V on Pt/WC. Again, there is a slight reduction in the mass transport limiting current whose origin is unclear; however, the large enhancement in the ORR activity certainly justifies further studies into this family of materials.

Finally, platinized WO_3 and WC were electrochemically cycled between 0.0 and 1.4 V 300 times at 10 mV/s. The results are presented in Figure 6. In both cases, the Pt cluster activity is significantly reduced following potential cycling. For Pt/WC, the onset and half-wave potentials shift negative, returning to the values observed for Pt/C, where no Pt-support interactions are active. This suggests that a significant portion of the

dx.doi.org/10.1021/cs100140s |ACS Catal. 2011, 1, 212–220

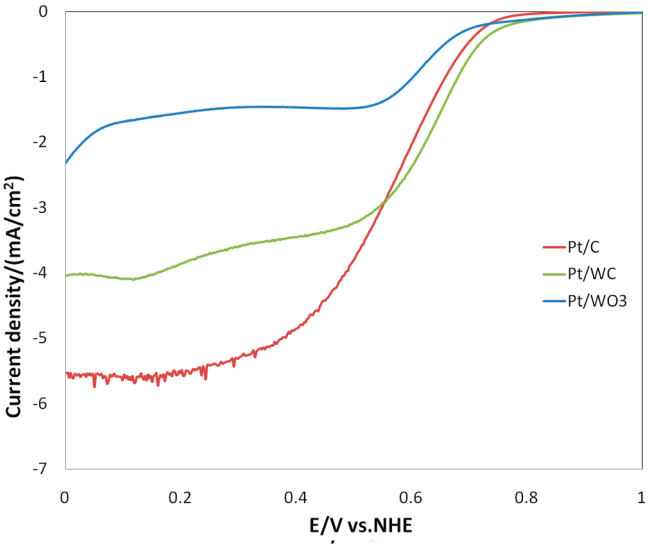

Figure 6. Linear sweep voltammograms for Pt/WC and Pt/WO_3 electrocatalysts on their 300th cycle compared with Pt/C in O_2-saturated 0.05 M H_2SO_4 at 1600 rpm; scan rate 10 mv/s.

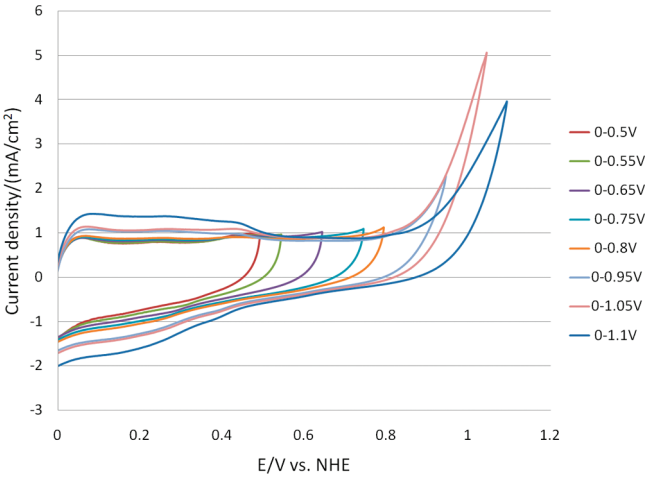

Figure 7. CVs for raw WC supports in N_2-saturated sulfuric acid.

WC-supported Pt became unaffiliated with the WC surface during cycling. The root cause for this was explored by both voltammetry of the WC supports, XPS, and TEM.

3.5. Electrochemical Stability of Raw and Platinized WC Supports. Cyclic voltammograms were obtained for raw WC supports in N_2-saturated 0.5 M H_2SO_4 at room temperature to investigate their redox stability at the potential window relevant for the ORR. First, the potential was cycled between 0.0 and 0.5 V. Then, for each subsequent experiment, the positive end of the potential window was extended by 50 mV. This was repeated until the threshold potential was 1.1 V. Figure 7 shows the results for the potential window opening experiments on the thin film WC electrode.

In the deoxygenated electrolyte, WC showed some activity for hydrogen adsorption/desorption between 0.0 and 0.35 V. Following the hydrogen region, the WC exhibited typical capacitive behavior until the onset of a strong irreversible oxidation current at around 0.85 V. This irreversible oxidation peak suggests that the WC support may be unstable at elevated potentials. In addition, integrating hydrogen adsorption charge between 0 and 0.35 V

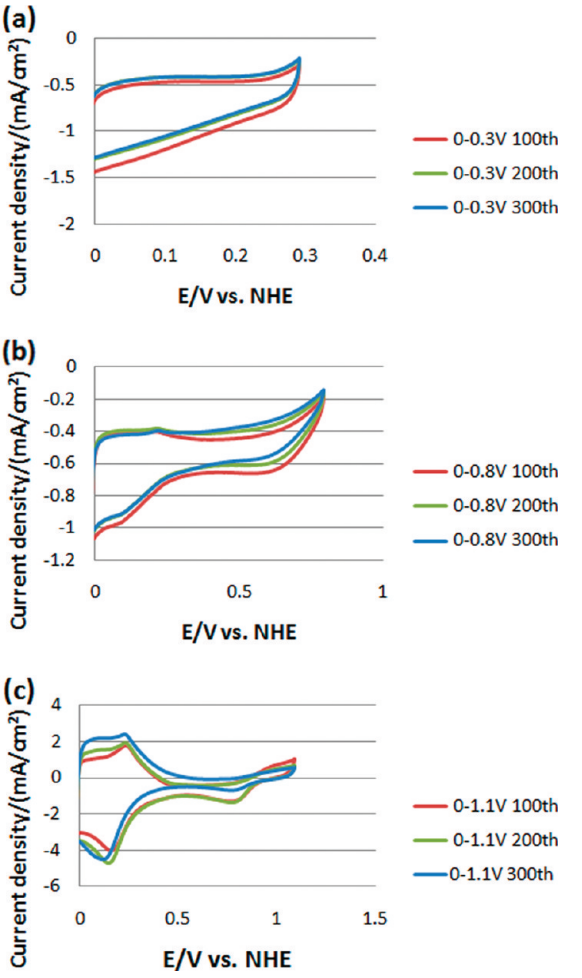

Figure 8. Cyclic voltammograms of Pt/WC in O_2-saturated 0.5 M H_2SO_4 between (a) 0 and 0.3, (b) 0 and 0.8, and (c) 0 and 1.1 V; scan rate = 10 mV/s.

shows a slight increase as a function of threshold potential. This is most likely caused by a slight roughening of the surface with potential treatment, which was observed by SEM (Supporting Information Figure S2) for WC cycled 300 times to 0.85 V. This roughening was not observed on samples whose potential was cycled below 0.8 V and appears to be a direct result of the oxidation reaction observed by CV.

Platinized supports were also investigated by potential opening experiments between 0.0 and 1.1 V in O_2-saturated electrolyte. At each potential, the electrocatalyst was cycled 300 times. CV results for several cycling windows are presented in Figure 8. At each potential, scans 100, 200, and 300 are reported. Figure 8a presents CVs with a threshold potential of 0.3 V. Here, the current remains in the negative regime during cycling due to the background ORR current, and there is no observable difference between the scans, suggesting stability for both Pt and the support below 0.3 V. Figure 8b shows equivalent data with a maximum cycling potential of 0.8 V. In this figure, a small deviation is observed between the scans. There is a slight decrease in the hydrogen adsorption/desorption current as well as a positive shift in the Pt surface oxidation current and a lowering of the magnitude and definition of the surface oxide reduction with increasing scancount.

Finally, Figure 8c shows the Pt/WC electrocatalyst cycled 300 times between 0.0 and 1.1 V. From this voltammogram, it is clear

dx.doi.org/10.1021/cs100140s |*ACS Catal.* 2011, 1, 212–220

that the Pt is well dispersed on the surface and all of the characteristics of the pure Pt voltammogram are observed. In addition, there is clear ORR activity, and the total current is shifted negative, and the double layer region is centered negative of zero. A significant change in the voltammogram is observed between 100 and 300 cycles. First, there is a clear increase in the hydrogen region, which was consistent with that observed on raw WC. In addition, the magnitude and definition of the Pt surface oxide formation and reduction diminished with increasing number of scans. This suggests that although the electrocatalyst support surface area is increasing with time, the Pt electrochemically active area is decreasing.

The Pt active area decrease is corroborated by TEM images collected for the platinized supports both without electrochemical cycling and Pt/WC cycled between 0.0 and 1.1 V. These are shown in Figures 9 and 10, respectively. Figure 9 shows that our synthesis method results in homogeneously deposited 3 nm Pt clusters on the support surface. However, Figure 10 shows that potential cycling results in two types of Pt structures on the surface. The first type was remaining 3 nm particles from the initial synthesis that showed good electrochemical stability. The second Pt architecture observed was very large agglomerates, ranging from 25 to 200 nm in size, that appear to consist of detached 3 nm Pt particles (Figure 10). It has been suggested that detached Pt particles can result from limited interaction between the catalyst and surface species,[47] such as unaffiliated C and WO_3. This Pt agglomeration is the most likely cause for the reduced Pt electrochemically active area observed in Figure 8c. This also explains the reduction in ORR activity, including the return of the onset and half-wave potential to the Pt/C values, after potential cycling reported in Figure 5. Clearly, the observed current response was dominated by these large agglomerates that are completely unassociated with the support. Thus, the metal−support interaction is still active on the remaining 3 nm particles bound to the WC; however, the instability of the support surface and limited interaction between Pt and non-WC surface species compromises the overall Pt cluster stability.

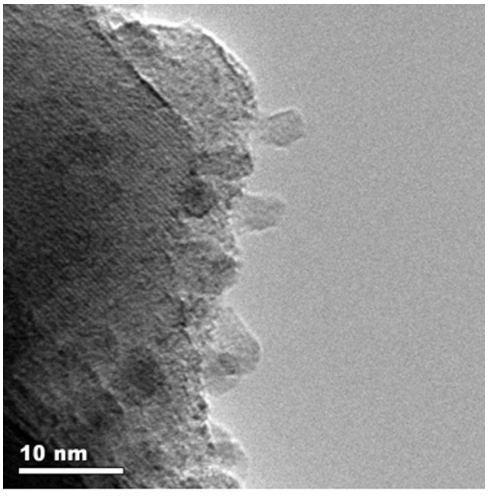

Figure 9. TEM image of platinized WC before cyclic potential experiments.

Finally, XPS was used to determine the change in surface composition as a function of electrode potential to elucidate the nature of the experimentally observed oxidation current at $E > 0.85$ V. The results for the XPS studies are presented in Table 3. Since the amount of non-WC surface carbon was constant for all experiments, it is not included in the calculation of values in Table 3. Two interesting features are observed. First, the surface W that covers the support following synthesis is oxidized to WO_3 and WO_2 species during platinization, which occurs in an acidic solution. Several possible reactions have been proposed in the literature; however, the most thermodynamically favored process is the oxidation of WC to tungsten(VI) oxide and CO_2 (eq 14).[48]

$$2WC(s) + 5H_2O(l) \rightarrow 2WO_3(s) + 2CO_2(g) \qquad (14)$$

Table 3. Surface Composition for Pt/WC Determined by XPS before and after Various Electrochemical Cycling

treatment	WC	W	WO_3	WO_2
as synthesized WC	19.6	48.7	23.6	8.0
Pt/WC	30.4		42.3	29.8
Pt/WC: 0.3 V	25.3		51.7	23.1
Pt/WC: 0.8 V	15.6		49.5	34.9
Pt/WC: 0.85 V	15.2		56.5	28.3
Pt/WC: 1.1 V	11.2		62.2	26.6

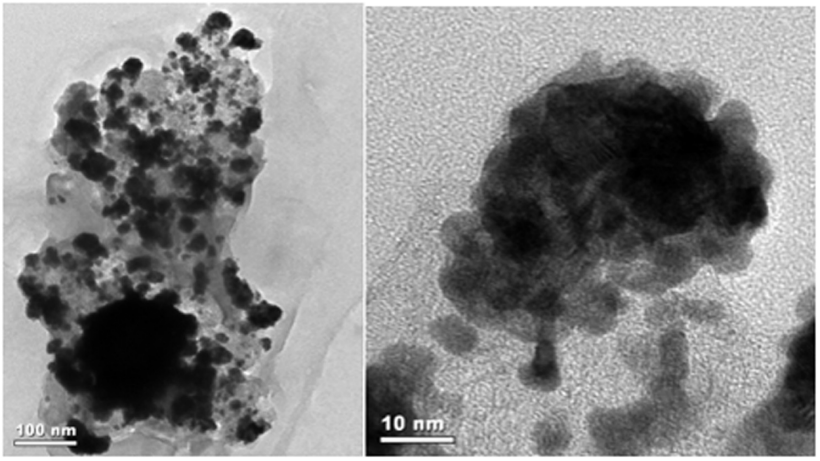

Figure 10. TEM image of Pt/WC after cycling between 0 and 0.8 V 300 times.

dx.doi.org/10.1021/cs100140s |*ACS Catal.* 2011, 1, 212–220

Second, it is clear from Table 3 that the final surface composition is a strong function of the maximum cycling potential, where the composition of WC decreases with increasing potential, while the surface oxide concentration increases with increasing potential. At low cycling potentials, < 0.3 V, about 17% of the surface WC is converted to WO_3, forming a redox-stable passivation layer on the support surface.[49] This layer allows the subsurface WC to maintain its structure for several hundred millivolts, which is apparent from the voltammetry results shown in Figure 7. However, at potentials >0.8 V, significant electrochemical oxidation of subsurface WC to WO_x occurs by eqs 15 and 16.[23,49,50]

$$WC(s) + 4H_2O \rightarrow WO_2(s) + CO_2(g) + 8H^+ + 8e^- \quad (15)$$

$$WO_2(s) + H_2O(l) \rightarrow WO_3(s) + 2H^+ + 2e^- \quad (16)$$

The electrochemical formation of WO_2 and WO_3 with cycling may also explain the surface roughening observed by SEM, where the new WO_x species grow in an amorphous phase from the WC sites.

Finally, the redox stability of commercially available WO_3 was investigated by CV in N_2-saturated sulfuric acid. The electrochemical signature of the WO_3, shown in Supporting Information Figure S3, is vastly different from WC (Figure 7). Here, the hydrogen adsorption/oxidation peaks are compressed, and there is no oxidation peak observed, even when the electrode is cycled to 1.4 V. This suggests that WO_3 is a stable surface species that will eventually populate the entire WC surface given sufficient reaction time.

CONCLUSIONS

WC electrocatalyst supports were synthesized in this study and investigated as support materials for Pt electrocatalysts. First, it was found that there exists a thermodynamic limitation for the formation of pure surface WC, where near-surface W and C atoms segregate to the surface and are subsequently oxidized when exposed to air or aqueous media. Second, it was observed that Pt clusters could be placed with high dispersion on the WC support surface. In addition, the electron transfer between Pt and the support enhanced the catalyst activity for the ORR significantly. However, it was found that the WC surface was unstable at potentials relevant to the ORR and formation of WO_x species causes both surface roughening and deformation, and also facilitates the detachment of Pt clusters from the support. This leads to large Pt agglomerates and eliminates the synergistic effect observed on as-prepared Pt/WC. Therefore, WC provides an interesting test bed for research because of its interaction with Pt and enhancement in its initial activity and dispersion, although it is not a viable long-term electrocatalyst support, and future work should focus on identifying materials that interact with Pt similarly with improved electrochemical stability.

ASSOCIATED CONTENT

Supporting Information. SEM and TEM Images, cyclic voltammograms and calculated Gibbs energies. This material is available free of charge via the Internet at http://pubs.acs.org.

AUTHOR INFORMATION

Corresponding Author

*Phone: 860-486-2756. Fax: 860-486-2959. E-mail: mustain@engr.uconn.edu.

ACKNOWLEDGMENT

This work was funded by the U.S. Department of Energy Office of Basic Energy Sciences, Grant No. DE-FG02-10ER16200. The authors also acknowledge the Institute of Materials Science and the Center for Clean Energy Engineering at the University of Connecticut for free use of the physical characterization equipment.

REFERENCES

(1) Nissinen, T. A.; Kiros, Y.; Gasik, M.; Leskela, M. *Chem. Mater.* **2003**, *15*, 4974–4979.
(2) Jaouen, F.; Marcotte, S.; Dodelet, J. P.; Lindbergh, G. *J. Phys. Chem. B* **2003**, *107*, 1376–1386.
(3) Weidenkaff, A.; Ebbinghaus, S. G.; Lippert, T. *Chem. Mater.* **2002**, *14*, 1797–1805.
(4) Forti, J. C.; Robledo, A. M.; Kokoh, K. B.; Andrade, A. R.; Vante, N. A. *Electrochim. Acta* **2006**, *51*, 2800–2808.
(5) Vu, T. N.; Gestel, J.; Gilson, J. P.; Collet, C.; Dath, J. P.; Duchet, J. C. *J. Catal.* **2005**, *231*, 468–479.
(6) Santori, G. F.; Moglioni, A. G. *Appl. Catal., A* **2004**, *269*, 215–223.
(7) Toukoniitty, A. E.; Nieminen, A. V.; Taskinen, A. *J. Catal.* **2004**, *224*, 326–339.
(8) Gangeri, M.; Centi, G.; Malfa, A. L.; Perathoner, S.; Vieira, R.; Huu, C. P.; Ledoux, M. J. *Catal. Today* **2005**, *102*, 50–57.
(9) Arico, S.; Srinivasan, S.; Antonucci, V. *Fuel Cells* **2001**, *1*, 133–161.
(10) Gasteiger, H. A.; Pane, J. E.; Yan, S. G. *J. Power Sources* **2004**, *127*, 162–171.
(11) Lee, J.; Lee, K.; Kim, S. H. *J. Power Sources* **2007**, *165*, 667–677.
(12) Mukerjee, S.; Srinivasan, S. *J. Electroanal. Chem.* **1993**, *357*, 201–224.
(13) Zhang, J.; Vukmirovic, M.; Xu, Y.; Mavrikakis, M.; Adzic, R. *Angew. Chem., Int. Ed.* **2005**, *44*, 2132–2135.
(14) Liu, H.; Xia, D.; Zhang, J. *Platinum-Based Alloy Catalysts for PEM Fuel Cells*; Zhang, J., Ed.; Springer: London, 2008.
(15) Meng, H.; Shen, P. K. *Chem. Commun.* **2005**, *1*, 4408–4410.
(16) Xu, C. W.; Zeng, R.; Shen, P. K.; Wei, Z. D. *Electrochim. Acta* **2005**, *51*, 1031–1035.
(17) Nie, M.; Tang, H. L.; Wei, Z. D.; Jiang, S. P.; Shen, P. K. *Electrochem. Commun.* **2007**, *9*, 2375–2379.
(18) Levy, R. L.; Boudart, M. *Science* **1973**, *181*, 547–549.
(19) Li, G. H.; Ma, C. A.; Tang, J. Y.; Sheng, J. F. *Electrochim. Acta* **2007**, *52*, 2018–2023.
(20) Li, G. H.; Ma, C. A.; Zheng, Y. F.; Zhang, W. M. *Microporous Mesoporous Mater.* **2005**, *85*, 234–240.
(21) Schlapbach, L.; Zuttel, A. *Nature* **2001**, *414*, 353–358.
(22) Wu, M.; Shen, P. K.; Wei, Z. D.; Song, S.; Nie, M. *J. Power Sources* **2007**, *166*, 310–316.
(23) Ham, D. J.; Lee, J. S. *Energies* **2009**, *2*, 873–899.
(24) Meng, H.; Shen, P. K. *J. Phys. Chem. B* **2005**, *109*, 22705–22709.
(25) Ganesan, R.; Lee, J. S. *Angew. Chem., Int. Ed.* **2005**, *44*, 6557–6560.
(26) McIntyre, D. R.; Burstein, G. T.; Vossen, A. *J. Power Sources* **2002**, *107*, 67–73.
(27) Ganesan, R.; Ham, D. J.; Lee, J. S. *Electrochem. Commun.* **2007**, *9*, 2576–2579.
(28) Baresel, D.; Gellert, W.; Heidemeyer, J.; Scharner, P. *Angew. Chem., Int. Ed.* **1971**, *10*, 194–195.
(29) Palanker, V. S.; Gajyev, R.; Sokolsky, D. V. *Electrochim. Acta* **1977**, *22*, 133–136.
(30) Nie, M.; Shen, P. K.; Wu, M.; Wei, Z.; Meng, H. *J. Power Sources* **2006**, *162*, 173–176.
(31) Chen, Y.-J.; Li, J. B.; Zhai, H. Z.; Wei, Q. M. *Mater. Lett.* **2002**, *56*, 279–283.
(32) Fleischmann, R.; Böhm, H. *Electrochim. Acta* **1977**, *22*, 1123–1128.

(33) Ross, P. N.; Macdonald, J.; Stonehart, P. *J. Electroanal. Chem.* **1975**, *63*, 450–455.
(34) Vidick, B.; Lemaitre, J.; Delmon, B. *J. Catal.* **1986**, *99*, 428–438.
(35) Chen, Y. J.; Li, J. B.; Zhai, H. Z.; Wei, Q. M. *Mater. Lett.* **2002**, *56*, 279–283.
(36) Rees, E. J.; Brady, C. D. A.; Burstein, G. T. *Mater. Lett.* **2008**, *62*, 1–3.
(37) Zhang, J.; Mo, Y.; Vukmirovic, M. B.; Klie, R.; Sasaki, K.; Adzic, R. R. *J. Phys. Chem.* **2004**, *108*, 10955–10964.
(38) Xiao, T.; Wang, H.; York, A. P. E.; Williams, V. C.; Green, M. L. H. *J. Catal.* **2002**, *209*, 318–330.
(39) Shrestha, S.; Mustain, W. E. *J. Electrochem. Soc.* **2010**, *157*, B1665–B1672.
(40) Har, Y.; Minami, N.; Hiroaki, I. *Appl. Catal., A* **2007**, *323*, 86–93.
(41) Giraudon, J. M.; Devassine, P. *J. Solid State Chem.* **2000**, *154*, 412–426.
(42) Esposito, V. D.; Dobson, K. D. *J. Electrochem. Soc.* **2009**, *156*, B962–B969.
(43) Ross, P. N.; Stonehart, P. *J. Catal.* **1977**, *48*, 42–59.
(44) Liang, C.; Ding, L.; Li, C.; Pang, M; Su, D.; Li, W.; Wang, Y. *Energy Environ. Sci.* **2010**, *3*, 1121–1127.
(45) Ragone, D. V. *Thermodynamics of Materials*; Wiley: New York.
(46) Knizhnik, A. A.; Safonov, A. A.; Iskandarova, I. M. *J. Appl. Phys.* **2006**, *99*, 84–104.
(47) Kundu, S.; Wang, Y.; Xia, W.; Muhler, M. *J. Phys. Chem. C* **2008**, *112*, 16869–16878.
(48) Andersson, K. M.; Bergström, L. *Int. J. Refract. Met. Hard Mater.* **2000**, *18*, 121–129.
(49) Weidman, M. C.; Esposito, D. V.; Hsu, I. J.; Chen, J. G. *J. Electrochem. Soc.* **2010**, *157*, F179–F188.
(50) Weigert, E. C.; Esposito, D. V.; Chen, J. G. *J. Power Sources* **2009**, *193*, 501–506.